

Master's thesis

2021

Master's thesis

Jonas Østergaard Støre

NTNU
Norwegian University of
Science and Technology
Faculty of Engineering
Department of Energy and Process Engineering

Jonas Østergaard Støre

The Effect of Arm Positions on Flow Around an Alpine Skier

June 2021



Norwegian University of
Science and Technology

The Effect of Arm Positions on Flow Around an Alpine Skier

Jonas Østergaard Støre

Mechanical engineering

Submission date: June 2021

Supervisor: Tania Bracchi

Co-supervisor: Ola Elfmark

Norwegian University of Science and Technology
Department of Energy and Process Engineering

Master`s Agreement / Main Thesis Agreement

Faculty	Faculty of Engineering
Institute	Department of Energy and Process Engineering
Programme Code	MTPROD
Course Code	TEP4925

Personal Information

Surname, First Name	Store, Jonas Østergaard
Date of Birth	07.07.1994
Email	jonasos@stud.ntnu.no

Supervision and Co-authors

Supervisor	Tania Bracchi
Co-supervisors (if applicable)	Ola Elfmark
Co-authors (if applicable)	

The Master`s thesis

Starting Date	15.01.2021
Submission Deadline	11.06.2021
Thesis Working Title	Flow topology and its effect on drag in the wake of an alpine skier
Problem Description	This thesis will look at flow topology in the wake of an alpine skier, and how it affects the aerodynamic drag. When an alpine skier is in the low tuck position or in the air after a jump, different arm position yield different aerodynamic drag results even though the frontal area is the same. This study will investigate the flow topology in the wake to better understand why this is. A 3D model of an alpine skier is printed with different arm positions to do measurements of different positions, and to be able to compare the findings. The tests are conducted by the use of the Large-Scale Wind Tunnel at NTNU. The scanning of the wake will be done using a cobra probe.

Comments to the Master`s Agreement

What was actually done in the master`s thesis differed some from the problem description written at the start of this semester. The frontal area was not the same for the different arm positions. Flow visualizations with use of oil were done to study flow separation points, and CFD simulations were completed as well to compare the experiment and validate a CFD model. In addition, force measurements and wake measurements were done for five different arm positions as described in the problem description attached.

Preface

This master's thesis was written at the Fluid Mechanics Laboratory and Wind Tunnel, Department of Energy and Process Engineering (EPT) at the Norwegian University of Science and Technology (NTNU) during the spring 2021. It was written as an article to make the thesis closer to a finished publication as this is the aim for the results obtained.

This study continues previous studies and research done by the Norwegian Olympic Committee (NIF), and is part of a larger project called Aerodynamics 2022. It is a collaboration between NIF and different Norwegian winter sports federations. The aim of the project is to give the Norwegian athletes a competitive advantage when it comes to clothing and techniques. The objective of this article was to do drag measurements, flow visualizations and wake measurements of different arm positions of an alpine skier in a wind tunnel. These results were compared to the results from CFD simulations with the aim to serve as validation for a CFD model being made by Nabla Flow. This is a company working with aerodynamics in sports, and they are developing a digital wind tunnel making simulations easier and available for more athletes. The Nabla Flow team is involved in the same project as this master thesis, and also other sports aerodynamics projects.

I would like to thank my supervisor Tania Bracchi for guidance through the year, for the discussions and the weekly meetings. I would also like to thank my co-supervisor Ola Elfmark for his continuous commitment and interest in my work from our first meeting in January 2020, for including me in his projects on sports aerodynamics and sharing his knowledge on the topic, and for always being available when needed. Knut Erik Teigen Giljarhus at the University of Stavanger also deserves my gratitude for pointing me in the right direction when needed, and for sharing his knowledge on sports aerodynamics, CFD and how to write a good paper. The PhD students at EPT, and especially Yannick Joos, deserves to be mentioned as well for helping with their knowledge on the wind tunnel and different measurement devices used. Finally, I would like to thank Sindre Wold Eikevåg for devoting his time to 3D print the model.



Jonas Østergaard Støre
9th of June 2021

The Effect of Arm Positions on Flow Around an Alpine Skier

Jonas Østergaard Støre ¹

¹Department of Energy and Process Engineering, Norwegian University of Science and Technology

There have been limited research increasing knowledge of flow around an alpine skier, and the effect of different arm positions. In this study, a wind tunnel experiment were conducted testing five different arm positions on a model of an alpine skier. Drag measurements were done, and the flow separation point was studied by doing flow visualizations with the use of oil and pigments. In addition, wake measurements were done with the use of a Cobra Probe. These results were compared to CFD simulations to serve as validation for a CFD model. The low tuck position was the best with regards to drag area, while the arms down along the legs position was the worst with 53% higher drag area than the low tuck position. The difference in drag area is due to smaller frontal area for the low tuck position, later separation point causing less pressure drop, and the forearms penetrating the air and bending the flow around the upper arms. This makes the low tuck position the most aerodynamic favorable position in this study. The experimental and simulation results coincided well offering further validation to the CFD model.

Key words: Aerodynamics in sports, alpine skiing, drag, CFD simulation, flow separation, wake measurements, wind tunnel

1. Introduction

On the topic of aerodynamics in winter sports, and especially alpine skiing, there have been done limited research increasing knowledge of flow around an alpine skier. Some studies have tested fabrics for the racing suits and the effect of skin suits and garments (e.g. Oggiano *et al.* 2013; Bardal & Reid 2012). Others have been done on the influence of snow friction compared to drag (e.g. Supej *et al.* 2012; Federolf *et al.* 2008), and a few studies on the forces in alpine skiing (e.g. Asai *et al.* 2016; Watanabe & Ohtsuki 1977; Savolainen & Visuri 1994). Aerodynamics on an alpine skier resemble bluff-body aerodynamics, where the flow around the body and in the wake is of particular interest when looking at the impact it has on the athletes. For a bluff body, pressure drag is the main drag component with only a smaller part coming from friction drag. The low tuck position is widely used in the high-speed disciplines of downhill (DH) and super-G (SG) to reduce drag. However, the flow structures around and behind the athletes are not well understood, and little has been published on the topic. This has not been an area of focus, and it is assumed that many teams keep the findings to themselves because it is the ideal way to try to gain an edge over other nations competitors.

Savolainen & Visuri (1994) found that in DH and SG, the aerodynamic drag force is in the magnitude of 80-90% of the total resistive force acting on the skier. Consequently, any reduction in drag can be hugely beneficial for the athletes. The drag force is defined as

$$F_D = \frac{1}{2}\rho U_{rel}^2 C_d A, \quad (1.1)$$

where ρ is the density of air, U_{rel} is the speed of the object relative to the fluid, C_d is the coefficient of drag and A is the frontal area of the skier. C_d is dependent on the Reynolds number, the surface roughness, and form of the body posture. The latter is something the athletes can affect for example with different arm positions. The Reynolds number is defined as

$$Re = \frac{\rho U_{\infty} D}{\mu} \quad (1.2)$$

where D is the characteristic length and μ is the dynamic viscosity. The characteristic length used for this paper is the shoulder width of the model as introduced by Elfmark, Reid & Bardal (2020). It was measured to $D = 48$ cm. From Equation (1.1) it is evident that the two variables one can influence to get lower drag force is the frontal area and drag coefficient as the velocity will be high in DH and SG, and the density is determined by ambient pressure and temperature. When doing experiments with athletes in sports aerodynamics, the experimental results are often presented as the product of C_d and A , and is known as aerodynamic drag area ($C_d A$). This variable is proportional to the drag force, but is more precise as velocity and density are accounted for, and it is difficult to measure the frontal area exact in such studies (Meyer, Le Pelley & Borrani 2011; Brownlie 2020; Elfmark *et al.* 2021; Crouch *et al.* 2014).

Much of the research that has been done on alpine skiing is with use of a wind tunnel. Watanabe & Ohtsuki (1977) published one of the first papers, and since then there have been done several articles on the topic (Supej *et al.* 2012; Barelle, Ruby & Tavernier 2004; Luethi & Denoth 1987; Elfmark & Bardal 2018; Elfmark, Reid & Bardal 2020; Elfmark *et al.* 2021). A huge advantage with a wind tunnel is the possibility of drag measurements with controlled variables yielding precise measurements. However, it is difficult to do wake measurements on real athletes as it is hard to keep the same posture for a long period of time and the probability of repeating the exact position could be somewhat low. As a consequence, a static model or a mannequin is convenient. It is even possible to do oil visualizations of the flow to see where the flow separates from the surface. Crouch *et al.* (2014) used a cyclist mannequin in time-trial position to conduct an experiment on pressure distribution, flow visualization and wake measurements. Asai, Hong & Ijuin (2016) used a model of an alpine skier made from steel core frames and a modified human mannequin. The study compared results from a wind tunnel experiment to computational fluid dynamics (CFD) simulations on a 3D model of a DH racer constructed from a laser scan. Their main focus were on the total drag, and which parts of the body that contributed the most to total drag. Elfmark *et al.* (2021) also conducted a study comparing experimental and simulation data to better understand the low tuck position in the speed disciplines.

When conducting experiments in a closed wind tunnel, the test subject will cause a significant blockage effect if the frontal area of the subject is large enough. As a consequence, the air is forced towards the top, bottom and side walls which could cause the flow to accelerate due to continuum mechanics as described by Maskell (1965). This

effect has to be corrected for comparing tests with different frontal areas, and to obtain results that coincide with what is actually happening during a race outdoors or in other wind tunnels with larger cross sections. The magnitude of the blockage effect depends on how large the object is. This is often measured as blockage ratio (B) which is defined as the frontal area of the test subject divided by the cross sectional area in the wind tunnel. Exactly how large B has to be to have an effect on the results is debated in literature. West & Apelt (1982) recommends anything above 6% for a cylinder in Re_d between 10^4 and 10^5 , while Carbó Molina *et al.* (2019) suggests blockage correction when the blockage ratio exceeds 10%. Battisti *et al.* (2011) proposed 5-10% as a high degree of blockage, and Anthoine, Olivari & Portugaels (2009) writes that blockage effects can be neglected with a ratio below 3%. This indicates that somewhere between 3% and 10% blockage could affect the results.

There are several methods to correct the results for blockage effects, and it is a topic that has been studied in a comprehensive manner. In this study, the formula Maskell (1965) suggested for correction in a closed test section wind tunnel has been used. It is defined as

$$\frac{C_{du}}{C_{dc}} = 1 + \theta C_{du} B, \quad (1.3)$$

where C_{du} is the uncorrected drag coefficient, C_{dc} the corrected drag coefficient, θ the blockage constant and B the previously defined blockage ratio. Elfmark & Bardal (2018) have previously estimated $\theta = 2.58$ with an aspect ratio of 3 when studying blockage on alpine skiers, while Maskell (1965) showed from experimental data that $\theta = 0.96$ for a bluff body with an infinite aspect ratio. In a later study, Elfmark, Reid & Bardal (2020) determined an optimal $\theta = 2.52$ for the low tuck position in alpine skiing. This was based on the least square residual fit between the results from two separate wind tunnels, and is used for this study.

Flow separates from the surface of an alpine skier when the boundary layer detaches into the wake. The point of separation affect the wake size which in turn affects the drag force due to a difference in pressure loss. As a consequence it can be used to interpret changes in drag values between objects with different separation points. When the streamwise pressure gradient is too large, low-momentum flow inside the boundary layer close to the surface separates. In the case of an adverse pressure gradient, $\frac{\partial P}{\partial x} > 0$, the velocity close to the surface is decreased, and the tangent of the velocity becomes flatter. At the point of separation, the velocity profile vanishes. The flow separates as it has to move against the increasing pressure force as well as the viscous forces. Then, the fluid particles will start to move in the opposite direction, called backflow, due to the external forces. The location of the separation point depends on several properties like the geometry of the object, Reynolds number and surface roughness, but is usually hard to predict (Anderson 2010).

The goal of this paper is to improve knowledge and obtain more information about the flow around an alpine skier, and also receive more data to validate a CFD model currently being made by Nabla Flow. The scope of this study is to investigate how different arm positions affect the drag forces on an alpine skier. In addition, this experiment will look at flow visualization by the use of oil and pigments for different arm positions to see where the flow separates on the arms. This gives an indication of wake size, and can be connected to the change in drag area values for the different arm sets. Wake measurements have been done to identify characteristics of the flow and large-scale wake structures. Acquiring more knowledge on flow around an alpine skier would be of great

interest for researchers, but also for the athletes and teams. As a consequence, the teams could improve the techniques used, and the equipment and ski racing suits. Especially when jumping, this could provide useful results for the athletes as the low tuck position is difficult to maintain. The wake measurements were limited to the low tuck position for this study due to time constraints. This is the most important position in alpine skiing and was preferred over other arm positions that will be introduced in Section 2.1. The arms were chosen as scope for this study as this is the body part that changes positions the most during a race, and hence, more detailed studies are needed. Finally, the data from the experiments have been compared to the data obtained by CFD simulations of the similar arm positions.

2. Method

2.1. Experimental set-up

The model used for these experiments was a 3D printed scan of a female top 10 world-ranked alpine skier from the Norwegian national team. The model was printed in full size from a 3D scan of the subject with use of PLA and PETG filament. It was manufactured with interchangeable arms. The arms made it possible to do measurements on different arm positions. Five different arms were printed; baseline position, arms down along the legs, arms out, hands behind the legs and hands behind the torso. An advantage with a printed model over real athletes is the possibility to make thorough measurements of the wake as the model maintains the same position all the time. The model with the different sets of arms is illustrated in Figure 1 with baseline being the typical low tuck position athletes used during competition. The other arm sets are three typical flight positions the athletes normally have during a competition when not able to maintain the baseline position, e.g. during a jump. In addition, one arm set with arms out in the flow was tested as this can happen when the athletes are out of balance or during turns.



Figure 1: The model without arms and head, and different arm positions tested in this study. From the left: Without arms and head, baseline position, arms down, arms out, hands behind ankles and hands behind torso.

The model of the alpine skier was mounted directly to a Schenck six-component force balance. The set-up in the wind tunnel is displayed in Figure 2 a). The velocity just upstream of the model was measured by the use of a Pitot tube.

The experiment was conducted in the large-scale wind tunnel at the Norwegian University of Science and Technology (NTNU), with a cross sectional area of 2.7 m x 1.8 m, and a length of the test section of 11.1 m. It is a closed-loop wind tunnel, and can reach velocities up to 23 m/s. The inflow is uniform, with a background turbulence intensity about 1%. The wind tunnel is equipped with a Pitot tube close to the area where the

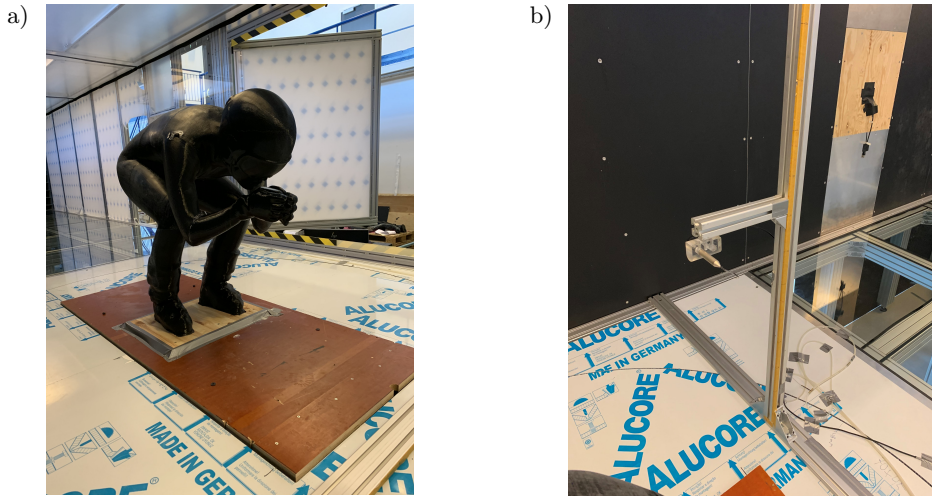


Figure 2: a) Set-up in the wind tunnel of the model in baseline position. b) Traverse used for the wake measurement with the Cobra Probe mounted to the end of an AluFlex beam.

model was mounted and a thermocouple for temperature measurements. These were used to calculate the Reynolds number (Re) of each flow velocity. The dynamic pressure and temperature were measured for each of the force measurements while the atmospheric pressure was measured from a mercury barometer.

The drag measurements were carried out at six different flow velocities between 10 m/s to 20 m/s with 2 m/s intervals for each of the five different arm sets. 20 m/s is slower than maximal the velocities the athletes are racing at in DH and SG. However, Elfmark, Reid & Bardal (2020) found 2-3% difference in C_dA between 20 m/s and 30 m/s. In addition, a more recent study by Elfmark *et al.* (2021) found similar results, justifying the use of lower test speed in the experiments for this study. Force data was sampled two times for each velocity. The sampling time used for the measurements were 30 seconds with a frequency of 2000 Hz. The final data used are the time-averaged data of the samples. The values of C_dA are calculated from the drag measurements as the velocity and density is known. The blockage effect was accounted for as all the arm positions had B between 5% and 7%. This study uses the method by Maskell, described in Equation (1.3), with a blockage constant $\theta = 2.52$ as Elfmark, Reid & Bardal (2020) suggested for the low tuck position.

The frontal area used to calculate the coefficient of drag was measured from the 3D scan used to print the model. The scan can be imported into any CAD software, and from these programs the frontal area is measured. To validate the results, a similar method to Elfmark & Bardal (2018) was used additionally. Pictures behind the 3D model were taken in front of a white wall, to create a sharp silhouette. The frontal area was calculated by counting black pixels from a binary image. A reference object with a known area was used to calculate a pixels per square meter calibration factor.

Flow visualizations were done by the use of an alloyed, mineral-oil-based monograde motor oil mixed with white pigments as the model was black. For the baseline position, the oil was applied to the arms, legs and back. The other arm positions from Figure 1 were tested with oil applied to the arms as this was the scope for the study. The tests were ran until the oil reached a static state on the model surface.

As the model is three dimensional, gravity will also be a factor of the final results. To avoid this having a large effect on the results, the wind tunnel was ready and running on low velocities while applying the oil. To ensure that the oil flow was primarily a result of wall shear stress, and because higher velocities are more interesting as described earlier in this section, the velocity was set to 20 m/s, equivalent to $Re = 6.35 \cdot 10^5$. In addition, the pictures were taken while the tunnel was still running on measurement velocity because gravity affected the final results shortly after turning the wind tunnel off making it very hard to see the flow separation points.

The wake measurements were done using a Cobra Probe from Turbulent Flow Instrumentation (TFI) connected to the data acquisition system and the TFI Device Control software, and a manually operated traverse. The Cobra Probe is a four-holed dynamic pressure probe, making it possible to measure 3-component velocity with the directions lying within 45 degrees of the probe axis. It also measures the turbulence intensity and pressure difference between the probe and the upstream static pressure. The traverse was made of an AluFlex beam spanning across the floor and another beam spanning from the floor to the roof as can be seen in Figure 2 b). The Cobra Probe was mounted to the vertical beam.

When mounting the 3D printed model to the force balance it was of great importance to orient the model as directly into the freestream flow as possible. Small changes in the angle towards the freestream flow can make considerably changes in the wake data. To ensure as good orientation as possible, several reference lengths from the foot to different parts of the wind tunnel were measured before the model was fastened.

Before conducting wake measurements, the Cobra Probe was calibrated and tested in freestream outside where the flow was affected by the model until the orientation of the probe was satisfactory. The results showed a change of freestream velocity below 1% compared to the Pitot tube, and a velocity in x and z direction below an absolute value of $|0.05|$ m/s, which is in agreement with Mallipudi, Selig & Long (2004). The pitch and yaw angle were kept below an absolute value of $|0.2|$ degrees. This calibration was done prior to each test day to ensure a correct orientation of the probe.

Originally, the plan was to do wake measurements for the entire wake for all the different arm sets to compare results. By doing this, it could be possible to present an explanation of why the drag forces are possibly different for the separate arm positions from a flow topology point of view. The wind tunnel was going through severe refurbishments at the time of testing, and was assembled temporarily for use by master's students. Hence, the new traverse was not mounted yet, and the traverse used in this study had to be operated manually. As this is time consuming and time in the wind tunnel was limited, it was decided to focus on the upper part of the wake for the baseline position at 20 m/s. The reason being that this area had generated the most interesting results from a previous CFD simulation of the low tuck position.

The grid used can be seen in Figure 3. The points were premarked on the beams before the test started. Data was sampled at points for each third cm in x and z direction from a plane $D/2$ behind the model yielding a total of 320 points. D is the shoulder width of the model. The sampling time used for each point was 30 s at 1280 Hz. The Cobra Probe was provided with uncertainties of ± 0.5 m/s and ± 1 degree pitch and yaw angles up to 30% of principal turbulence intensity (I_{uvw}). The manual also stated that the results above $I_{uvw} = 30\%$ yields good results. Draskovic (2017) investigated the accuracy of different measurement methods in complex turbulent flows. He compared the Cobra Probe to laser Doppler anemometry and hot wire anemometry, and found the probes fitting for such flows.

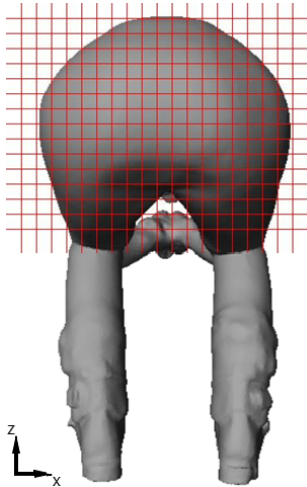


Figure 3: Measured grid of upper wake. Each sample point separated with 3 cm. in x and z directions.

2.2. Simulation set-up

The CFD simulations were performed using AeroCloud, a web-based service for aerodynamic simulations using cloud computing, developed by Nabla Flow (NablaFlow). The digital wind tunnel is a state-of-the-art high-performance computing tool with the aim of complementing experiments in the future. It is possible to obtain more data from a CFD simulation, and one can do parametric studies without the athlete present. For the alpine skiers this would mean spending less time in the wind tunnel. It would be sufficient with a laser scan similar to the one in this study to test different positions and receive feedback on what is the most beneficial regarding drag.

The 3D scan is imported through the web interface created where one decides the freestream velocity and how fine the mesh around the model should be. Finer mesh yields better results, but considerably larger computing time. The file is uploaded to the server conducting the simulation. Forces and coefficients, cumulative drag force and pressure distribution around the model is available from the server. In addition, there is a graphical interface where one can slice the model at different locations to obtain the u , v and w velocity components, and where vorticity is calculated.

The simulations were done for the five different arm positions displayed in Figure 1 at $U_\infty = 20$ m/s. Drag results were obtained with pressure distribution around the different postures as well, making it possible to see where the flow separates in the simulation. The digital wind tunnel assumes isotropic turbulence for the turbulence model, presenting a simplified version of the flow separation. In addition, wake data were obtained for the baseline model at the same location as the wake measurements with the Cobra Probe as described in Section 2.1. The wake results from the simulation were interpreted using ParaView, making it possible to compare experimental and simulation data.

3. Results

The results will be presented in separate sections containing drag measurements, flow separation points and wake measurements. The experimental and simulation results will be presented together for the different sections, and compared and discussed in Section 4.

First, frontal area measurements, drag coefficients and drag area is introduced before and after blockage corrections. Then, the flow separation points for the different arm positions are inspected. For the experiment, these results originates from flow visualization with oil. The simulations provided a pressure distribution around the model making it possible to determine the point of separation. Finally, wake measurements are presented with vector plots of velocity components with vorticity, and contours of the streamwise velocity component relative to the freestream velocity and turbulence intensity. In this study, the streamwise direction of the flow is defined as y direction. The plane perpendicular to the streamwise direction, looking directly at the model, is the xz plane as illustrated in Figure 3. The wake measurements in the wind tunnel were captured at a distance of $D/2$ behind the model in the low tuck position, where D is the shoulder width of the model. The results from the CFD simulation were obtained at the same distance behind the model making it possible to compare the results from the wind tunnel experiment and simulation.

3.1. Effect of arm position on drag

Table 1 illustrates the results from both the experimental measurements and simulations. The measured frontal areas, drag coefficients, uncorrected drag areas and blockage corrected drag areas are included for the different arm positions at $Re = 6.35 \cdot 10^5$. It is calculated from the measured temperature, calculated density and $U_\infty = 20$ m/s using Equation (1.2). The findings for this velocity are the most important as it is the closest one to maximal competition velocities as described in Section 2.1. The blockage corrected results are computed from Equation (1.3).

Table 1: The results for experimental and simulation drag measurements. Experimental frontal area (A), experimental corrected drag coefficient (C_{dc}), experimental uncorrected drag area ($C_{du}A$), corrected experimental drag area ($C_{dc}A$), simulation frontal area (A), simulation drag coefficient (C_d) and simulation drag area (C_dA).

Arm position	Experiment				Simulation		
	A [m ²]	C_{dc} [-]	$C_{du}A$ [m ²]	$C_{dc}A$ [m ²]	A [m ²]	C_d [-]	C_dA [m ²]
Baseline	0.266	0.621	0.179	0.165	0.263	0.581	0.153
Arms down	0.329	0.766	0.285	0.252	0.323	0.714	0.231
Arms out	0.340	0.662	0.251	0.225	0.333	0.607	0.202
Behind ankles	0.299	0.692	0.232	0.210	0.291	0.620	0.181
Behind torso	0.293	0.601	0.196	0.180	0.284	0.540	0.153

Experimental drag measurements were also done for $U = 10, 12, 14, 16$ and 18 m/s. The findings for the equivalent values of Re are summarized in Appendix A with Figure 4 illustrating how the corrected C_dA changes with Re and the different arm positions. As one can see from Figure 4, the drag area of the model is Reynolds dependent. This coincides well with the findings of Elfmark, Reid & Bardal (2020) for approximately the

same range of Re . Their research illustrates how C_d becomes Reynolds independent from around $7.30 \cdot 10^5$. However, there are little change in C_d between $6.50 \cdot 10^5$ and $7.30 \cdot 10^5$. As the $Re = 6.35 \cdot 10^5$ used in this section is somewhat lower than what Elfmark, Reid & Bardal (2020) found, the drag area is not Reynolds independent, but the change in $C_{dc}A$ are small for higher values of Re . The frontal area remains constant for all the velocities in this study. Hence, it is possible to compare the Reynolds dependency of $C_{dc}A$ in this study to C_d values obtained by Elfmark, Reid & Bardal (2020). Figure 4 illustrates that for the higher values of Re the change in $C_{dc}A$ is less than for the lower values of Re agreeing with the results from Elfmark, Reid & Bardal (2020).

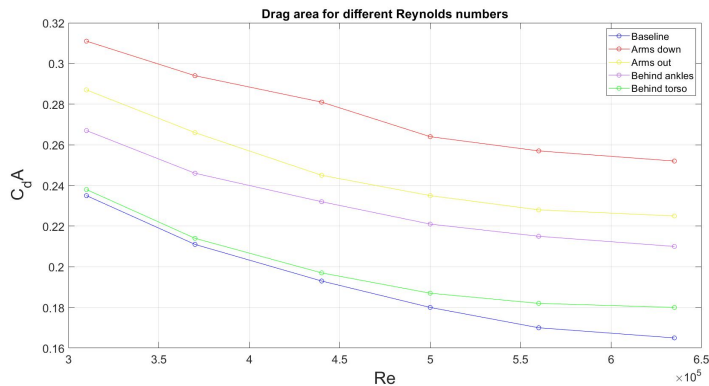


Figure 4: Corrected drag area ($C_{dc}A$) for the measured Reynolds numbers for all the arm positions.

Figure 5 shows a comparison of the drag area values for the other arm positions relative to the baseline position. The baseline position is the position yielding the lowest drag area, while the arms down along the legs provides the highest value for both the wind tunnel experiment and the CFD simulations.

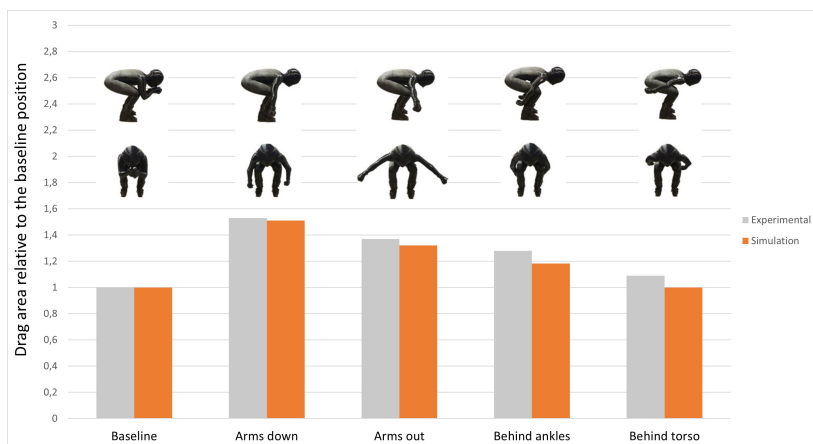


Figure 5: Corrected drag area ($C_{dc}A$) of the different arm positions relative to the baseline position for $U = 20$ m/s for the experiment (gray) and simulation (orange).

3.2. Flow separation point

The baseline position has results from arms, torso and thighs while the other arm sets have results from arms. The section contains visuals of the flow separation point for both the experiment and simulation. For the experiment, the separation point is the point furthest back of the areas where the oil is thicker and more concentrated. Pressure distribution around the model in different arm positions is used when looking at the flow separation point for the simulations. The blue areas indicates low pressure regions on the surface. The separation point is the point furthest back of these blue areas, where the colour becomes turquoise and hence, pressure is higher.

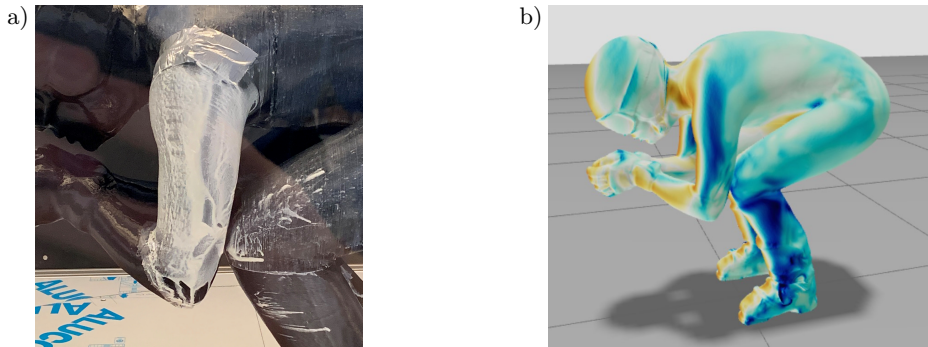


Figure 6: a) Flow visualization of the upper arm in baseline position. b) Pressure distribution around the baseline position from the simulation.

In the baseline position, separation occurs approximately on the middle of the arm as can be seen in Figure 6 a). At the height of where the triceps is touching the knee, one can see separation lines going towards the knee. These separation lines in the streamwise direction continues in an arc along the thigh as depicted in Figure 7 a) and b). There are some strips of oil angled behind the flow separation point at knee height which could indicate two separation points, but it is not clear from the experiment if this is the case. This phenomenon shows more clearly for other arm positions presented later in this subsection. The separation point for the simulation of the baseline is behind the center of the upper arm. A later separation point occurs around where the knee touches the upper arm, seen in Figure 6 b). At the point where the knee touches the arm, a flow separation point is observed on the upper part of the knee. This point extends to a line which ends a small distance above the knee. This follows the later separation point of the upper arm. The oil on the torso shows how the air moves from over the upper back

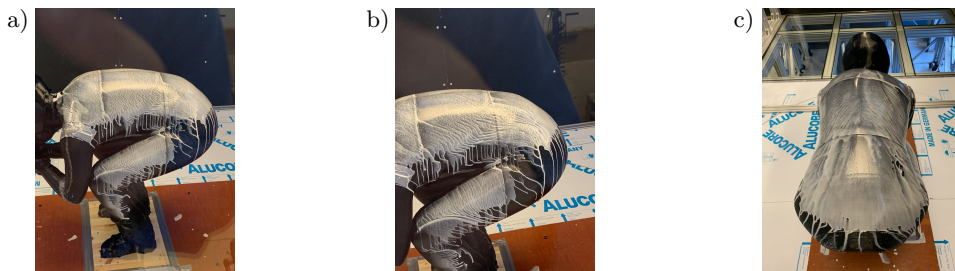


Figure 7: a) Side view of baseline position. b) Thighs in baseline position. c) Back view of baseline position.

towards the side of the hips on the lower back region. This is illustrated in Figure 7 b) and c).

Figure 8 a) shows where the air separates from the arms when held down along the legs. The air flowing past the upper arm separates at approximately the middle of the arm. The flow separation of the lower arm occurs earlier, and is located between the front and the middle of the arm. The point of separation for the upper and lower arm changes around the elbow. Figure 8 b) illustrates a separation point behind the middle of the upper arm from the simulation. This changes right above the elbow, with separation for the elbow and lower arm being earlier. The colour of the upper arm is notably dark blue, almost black, which indicates low pressure areas. This implies higher pressure drag as the pressure drop is larger.

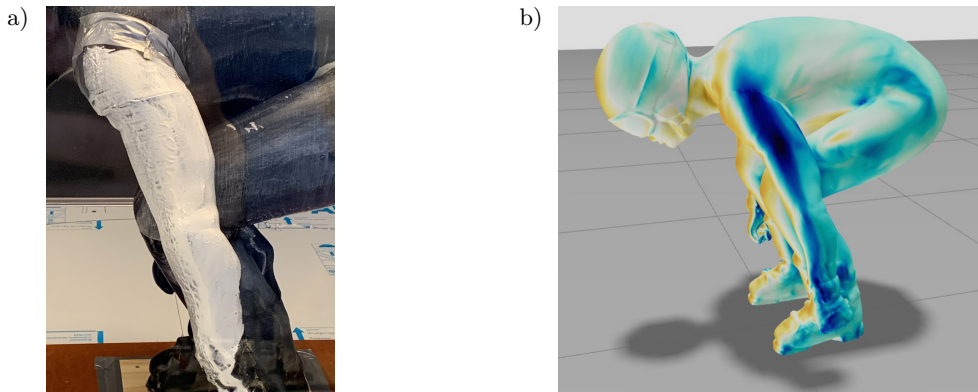


Figure 8: a) Flow visualization of the arms down position. b) Pressure distribution around the arms down position from the simulation.

For the arms out position, Figure 9 a) illustrates how the flow separates in the experiment. The separation points follow a somewhat straight line from the shoulder and down to the wrist. This line is somewhere between the middle of the arm and the front, indicating an early separation. From the simulation, Figure 9 b) shows a separation point behind the middle of the upper arm. This changes right above the elbow, with separation for the elbow and lower arm being somewhat earlier than for the upper arm.

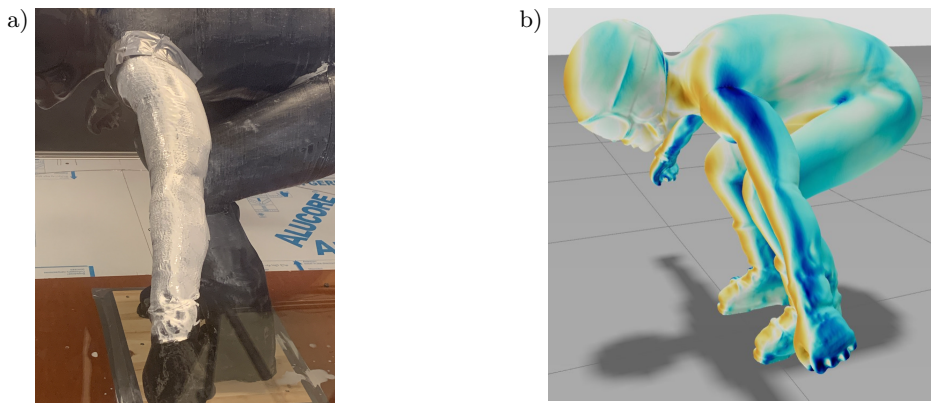


Figure 9: a) Flow visualization of the arms out position. b) Pressure distribution around the arms out position from the simulation.

Figure 10 a) displays where the flow separation occurs on the upper and lower arm when the hands are positioned behind the ankles. This arm position shows what looks like two different separation points on the upper arm indicating both laminar and turbulent separation, which will be discussed thoroughly in Section 4. The lower arm has an early separation located approximately around the ulna bone, straight towards the side wall of the wind tunnel. For the simulation of the hands behind ankles position, Figure 10 b) shows how the flow separates. The upper arm has a late flow separation, and this continues along the lower arm as well. The lower arm is also of a darker blue colour, indicating lower pressures than for the upper arm. The whole arm has a notably dark colour which means the pressure drag is having a considerably effect on the arm position as the pressure drop is large.

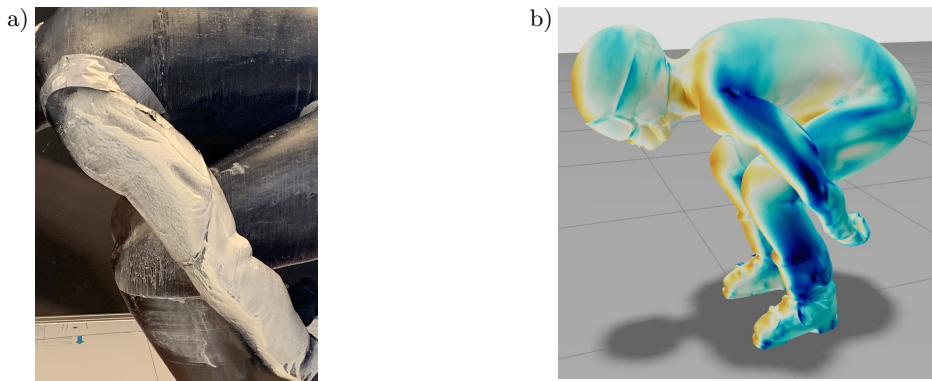


Figure 10: a) Flow visualization of the hands behind ankles position. b) Pressure distribution around the hands behind ankles position from the simulation.

The flow over the upper arm separates later for the wind tunnel test of the hands behind torso position as depicted in Figure 11 a). As for the hands behind ankles position, it seems to have two separation points just above and below the elbow. This is described in detail in Section 4. For the upper arm, the location of the latest flow separation point is so far back that it is pointing towards the roof of the wind tunnel. For this arm position as well, the flow separates earlier for the lower arm as Figure 11 b) illustrates. Finally, the hands behind torso position is considered for the simulation. Figure 11 c) displays a light blue colour for the upper arm making it harder to see where the flow separates. When studied in detail, the figure illustrates a considerably late separation point for the upper arm. This changes somewhat for the lower arm, once again having an earlier separation point. From the elbow the flow separates around the center of the arm. As the blue colour is light blue everywhere expect at the elbow the pressure drop for this position is smaller yielding lower pressure drag.

3.3. Classification of characteristic flow regimes

Figure 12 a) displays time-averaged contours of the streamwise velocity component relative to the freestream velocity $U_\infty = 20$ m/s from the wind tunnel experiment, while Figure 12 b) shows the same from the CFD simulation. Figure 12 a) shows that the wake is not symmetric, and one can identify primarily two low-velocity areas located behind the armpits and buttocks at $x = 12$ cm, 38 cm and $z = 60$ cm. The figure also shows a small strip of lower velocities at around $x = 35$ cm from $z = 75$ cm to $z = 90$ cm. This comes from the head and helmet. As can be seen from Figure 12 b), there are two larger,

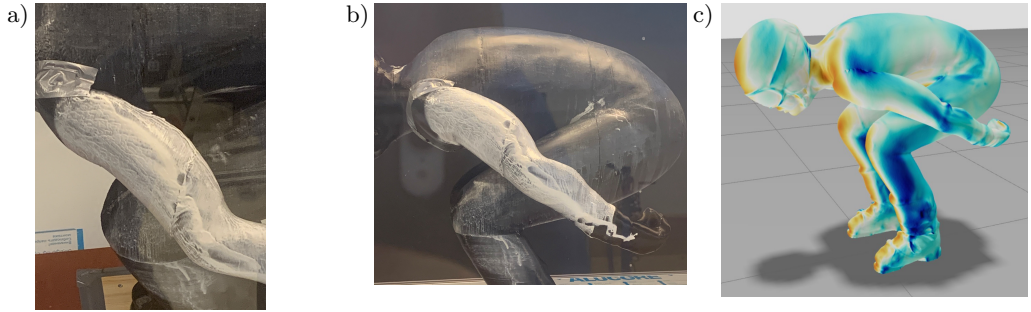


Figure 11: a) Flow visualization for the upper arm of hands behind torso position. b) Flow visualization for the lower arm of hands behind torso position. c) Pressure distribution around the hands behind torso position from the simulation.

blue areas right above the middle of the figure where the right one is located higher. These are areas with low velocity compared to the freestream velocity. This is assumed to come from the separation from the lower back, thighs and hips of the model. Above these areas there is a small white strip going towards the right. This is an area with lower velocities as well. This comes from the helmet and head. Two smaller, light blue areas are observed on the lower part of the figure. This indicates lower velocities that may be explained by separation around the legs.

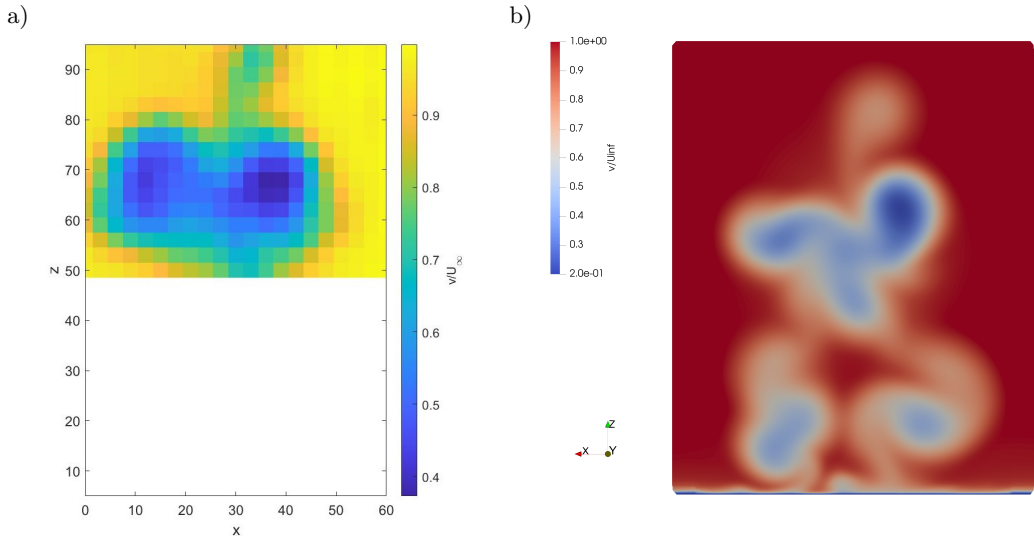


Figure 12: a) Contours of the streamwise velocity component (v) relative to the freestream velocity (U_∞) from the wind tunnel experiment. b) Contours of the streamwise velocity component (v) relative to the freestream velocity (U_∞) from the CFD simulation.

Figure 13 a) illustrates the principal turbulence intensity defined by $I_{uvw} = \frac{\sqrt{\frac{1}{3}(u'^2 + v'^2 + w'^2)}}{U_\infty}$. This figure is not symmetric either, and one can identify two high-turbulence areas located behind the armpits and buttocks at $x = 12$ cm, 38 cm and $z = 60$ cm. The figures also shows a small strip of higher turbulence at around $x = 35$ cm from $z = 75$ cm to $z = 90$ cm. This comes from the head and helmet. The areas

with high turbulence intensity coincide well with areas of low velocity from Figure 13 a). Figure 13 b) illustrates the turbulence intensity from the simulation, calculated from $I_{uvw} = \frac{1}{U_\infty} \sqrt{\frac{k}{1.5}}$ as the simulation provided the value of turbulent kinetic energy (k). Areas with higher turbulence intensity coincides well with the lower velocities from Figure 12 b). The brightest red areas just above the center with the highest I_{uvw} is assumed to come from the separation over lower back, hips and thighs, and the small white strip above from head and helmet. The smaller red areas towards the bottom of the figure are assumed to come from the legs.

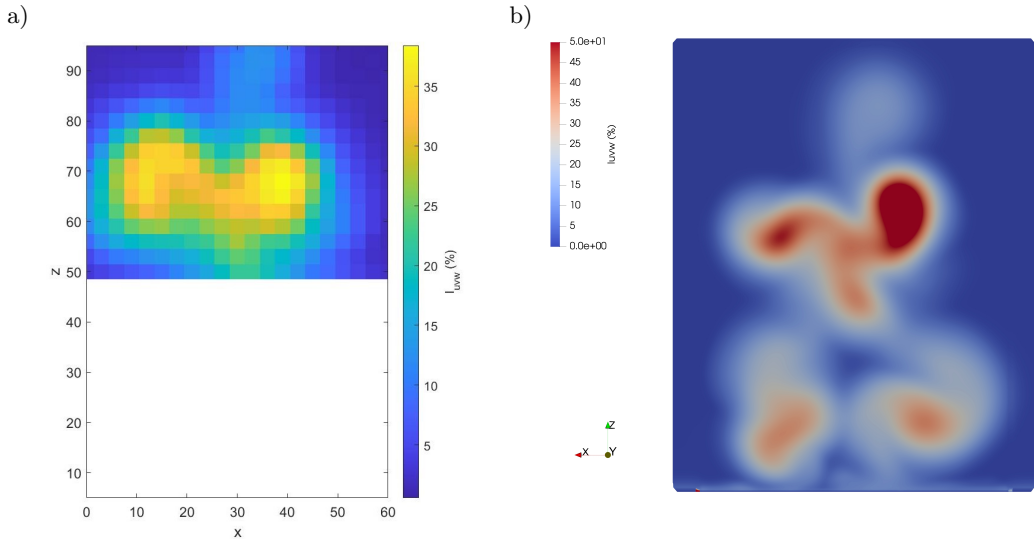


Figure 13: a) Contours of the principal turbulence intensity (I_{uvw}) from the wind tunnel experiment. b) Contours of the principal turbulence intensity (I_{uvw}) from the CFD simulation.

3.4. Identification of large-scale wake structures

Figure 14 a) shows a vector plot of the u and w velocity components in the xz -plane behind the model in the low tuck position. The vector plot displays which direction the flow is moving in. Contours of the vorticity is included as well to identify the areas of large positive and negative values of vorticity. Together, these results are used to define the large-scale streamwise vortices for the time-averaged flow. These structures account for the major separated flow regions in the wake of the model. As a consequence, it has a large effect on drag for the different arm positions. The vorticity (ω) is found by calculating the curl from the flow velocity, $\vec{\omega} \equiv \nabla \times \vec{u}$.

In Figure 14 a), two large counterclockwise rotating (CCW) vortices are identified in red. One above the right side of the back at $x = 35$ cm and $z = 68$ cm, and one around the left side of the hip at $x = 12$ cm and $z = 57$ cm. A larger clockwise rotating (CW) vortex is also identified at the left side of the back at $x = 21$ cm and $z = 66$ cm, with a smaller one located on the right side of the hip at $x = 39$ cm and $z = 57$ cm marked with blue. Such vortices are major contributors to pressure drag, which is the main drag component on an alpine skier with only a smaller part coming from friction drag.

Figure 14 b) shows a vector plot of the u and w velocity components, and the calculated

vorticity from the simulation. Positive values of vorticity are marked with red, and negative values with blue. Looking at the upper half of the figure, one can identify two large, red circles with CCW vortices. There are also CW vortices identified with blue, one larger below the red on the right side, and a smaller located higher to the left. Right below the blue CW vortex located on the right side there is a smaller red CCW vortex located in the middle. When looking at the lower half of the figure, it is evident that there are two blue CW vortices with large negative values. Right above the CW vortex to the lower right is a CCW vortex in red.

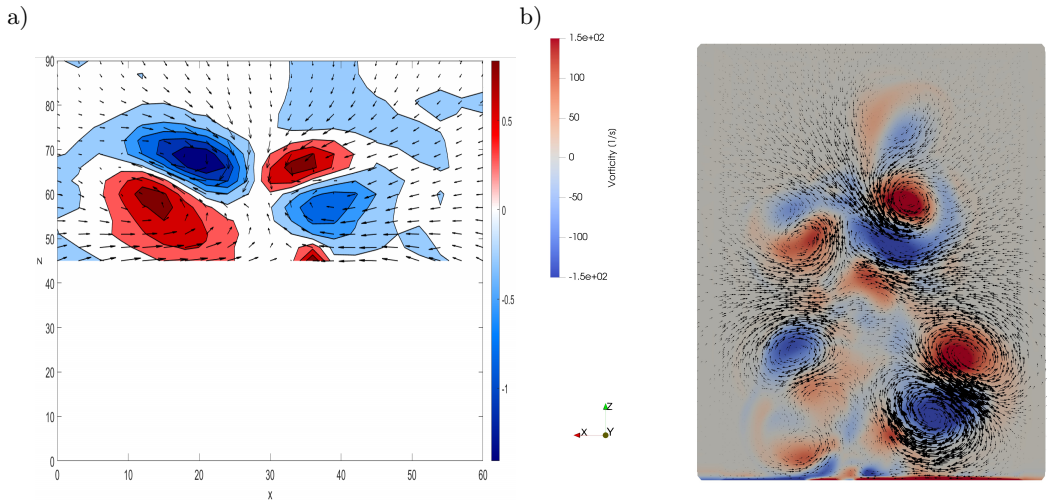


Figure 14: a) Vector plot of u and w velocity components with vorticity from the experiment. b) Vector plot of u and w velocity components with vorticity from the simulation.

4. Discussion

Table 1 displays that the baseline position from Figure 1 is the most beneficial when trying to keep a low drag area. From an aerodynamic perspective, it will be beneficial for the athlete to maintain the low tuck position for as long as possible during a competition. The drag area for baseline position, $C_{d_c}A = 0.165$, coincide well with the value obtained from a previous experiment ($C_dA = 0.167$) by Elfmark *et al.* (2021), further supporting the findings in this study with a 2% difference. The 3D scan used in the current study is of the same person as the test subject used by Elfmark *et al.* (2021). The arm position with arms extended along the lower legs should be avoided during a race as this provides the highest value of C_dA . It is evident that it is actually better to have the arms out from the body instead of having them straight down with the hands outside the legs. This is an interesting result as many of the athletes often end up in the arms down position as can be seen in Figure 15 a). It is the position many athletes seek to when not able to keep the hands in front during a jump as this is assumed to be a good flight position. The low tuck position is rarely used when jumping as it is difficult to keep the position during flight because of the forces present and as the hands are used to maintain the balance, but also due to lack of knowledge. Results from this study show that for all the velocities tested, the hands behind the ankles is the best alternative if assuming the

baseline position is not possible to hold. It is just as difficult to keep the arms down position as the hands behind ankles position, but the latter yield significantly better drag results as can be studied in Table 1 and Figure 4. This is an important result as it would be a small change in flight position for the alpine skiers, and could save them time during a competition. The hands behind ankles position is illustrated in Figure 15 b). As described in Section 3.1, $Re = 6.35 \cdot 10^5$ where these results were obtained at, is not Reynolds independent. However, the Re is close to independence as mentioned in 3.1, indicating that the results would not differ much for maximal competition speeds from what is obtained in this study. Figure 4 shows that the ranking of the best arm positions stays the same for all Re , implying correct results for higher Re as well. Higher Re might influence the flow separation point of the arm positions, but probably to a small extent as Re used for these results are close to Reynolds independence.

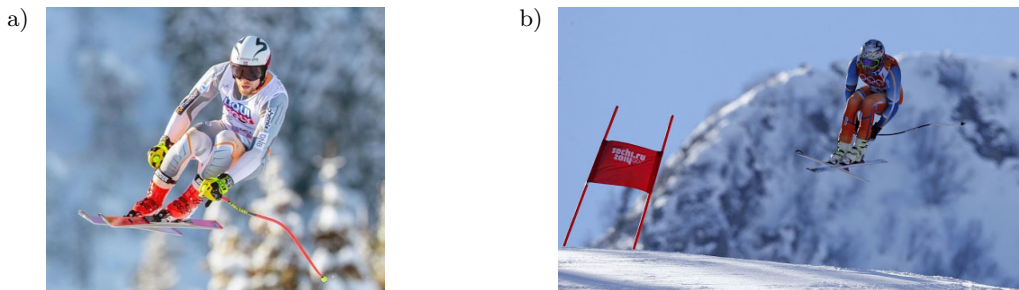


Figure 15: a) Last years world cup winner during a jump with arms down. Image credit: Getty Images. b) Former world and Olympic champion in a rare case of jumping with hands behind the ankles. Image credit: Reuters/Stefano Rellandini.

Another interesting feature of Table 1 is when looking at the drag area with respect to the measured frontal area and drag coefficient. One can see that the position with hands behind the torso actually is the most aerodynamic favorable position, yielding the lowest drag results. However, when holding this position, the frontal area becomes larger compared to the baseline position yielding higher values for drag area. Similarly, holding the arms straight out yield better results for drag coefficient than when the hands are behind the ankles. The increase in frontal area following the change of position means that that hands behind the ankles is the preferred position of those two.

The difference in drag area between baseline and the other arm positions is actually larger during a race as well. The reason for this is the change in how upright the athletes are in these positions, i.e. adjusted knee and hip angles. The model used for this study is printed from the baseline position with interchangeable arms. This was done in order to focus on how much the arms affect drag. When the alpine skier was scanned in the actual arms out and down positions she was more upright in the upper body which yields a larger frontal area and a less aerodynamic favorable position. In addition, for the arms down position, the athletes generally keeps the hands and arms closer to the legs than what is the case for this study. Humans are flexible and able to keep the arms close to the legs, something that is not possible when 3D printing. This could increase drag as well as the flow has to move around the arm with less space being available between the legs and arms.

Comparing flow separation points in Section 3.2 to Table 1, the findings support what has been discussed about the correlation between drag values and wake size. The hands behind torso position in Figure 11 a) illustrates the latest separation point of all arm

positions. Late separation yield a smaller wake resulting in lower pressure drop and hence, smaller drag values. This is the arm position with the lowest coefficient of drag from Table 1. When looking at the two arm positions with highest C_d from Table 1, Figure 8 a) and 10 a), it is clear that the earliest separation comes from the arms down position yielding the highest pressure drag of the two. One of the reasons for this is the increased wake size. It is not just the frontal area that makes the baseline position the better with regards to drag area compared to the hands behind torso position. When the forearms are placed directly into the flow, they penetrate the air as well, and resembles the front of more streamlined bodies. The forearms bends the air around the upper arms, compared to other arm positions where the flow hits the upper arm first.

It is hard to determine exactly which arm set that has the earliest separation when comparing some of the pictures. The arms down and out positions in Figure 8 a) and 9 a) have separation points in the same area on the upper arm and is difficult to separate. However, the flow separation point of the forearm is different between the two. It is clear that the arms down position has an earlier separation and hence, larger wake. This coincides well with drag data as it has a higher drag coefficient. The flow separation point is one of the reasons why different arm positions provide different drag values. An earlier separation yields a larger wake which increases the pressure drop. This causes higher pressure drag, and is important when studying an alpine skier as the pressure drag is the main drag component which is described in Section 1.

It is clear from Figure 10 a) and b), and Figure 11 a) and b) that both the hands behind ankles and hand behind torso positions have two flow separation points. This could indicate that first the laminar separation occurs. Then the flow experiences turbulent reattachment to the surface before the turbulent separation happens at the last flow separation point. This implies that the flow is in the critical region. If one assumes this to be flow around a cylinder with characteristic length the diameter of the arm, then $Re = 3.40 \cdot 10^5$. As per Zdravkovich (1997), Achenbach (1971), Achenbach (1975) and Bearman (1969), it is in the region of critical flow which has laminar separation, turbulent reattachment and turbulent separation present. Both arm sets have inclined arms downstream from the shoulder, and the findings indicate that this affects the flow separation. None of the other three arm sets display this phenomenon as clear as these two, even though the baseline position has some areas of interest where it is difficult to see exactly what happens behind the clear separation line.

When considering the flow separation point, one should discuss the surface roughness as it is an important property of where the flow separates. All the arm sets in this study had the same surface roughness, and is comparable. The model was printed with a nozzle size of 1 mm with 0.5 mm layer height in order to obtain as smooth surface as possible. Due to limited time between receiving the model and the test week in the wind tunnel, it was not time to treat the surface of the different arm sets to make the surface even smoother. The back and thighs of the model was polished with sandpaper as it was received before the arm sets.

As the arms down and arms out position are more or less the same position with the arms pointing in different directions it is interesting to look closer at why the drag area values are different. The first that is easy to point out is the difference in frontal area. The arms down position has a considerably larger frontal area as seen in Table 1. It also has an earlier separation as previously discussed and shown in Section 3.2. In addition to this, it is interesting to discuss how the flow behaves differently. For the arms down position, the arms are tight to the legs yielding an accelerated flow around the legs which would also have an effect on drag. Studies with two cylinders side-by-side have revealed different results regarding drag in such an arrangement. For small spacing between the

two cylinders, which is the case here between arms and legs, Zdravkovich & Pridden (1977) showed that the sum of the drag for the cylinder pair was always less than twice of a separate cylinder. However, Zhou *et al.* (2001) and Hori (1959) found the opposite, that the drag for the two cylinders side-by-side had a higher drag value than two separate added together due to an increase in interference drag. Biermann & Herrnstein Jr. (1933) measured drag at $Re = 6.5 \cdot 10^4$ and found that the drag was highest when the two cylinders were at a distance apart of 0.05 times the cylinders diameter (D), and lowest at $0.3D$ which supports that closer arrangements yield higher drag. The contradictions of the different articles makes it difficult to say something definitely about the effect of interference drag in the experiment for this paper. What is clear is that the drag is higher for the arms down position which is close to two cylinders side-by-side, than for arms out. For the latter, the distance between the arms and legs are large, implying that the interference drag is negligible.

Figure 12 a) and b), and Figure 13 a) and b) displays several interesting features. The small strip of lower v/U_∞ and higher I_{uvw} between $x = 27$ cm and 42 cm, and $z = 78$ cm and 90 cm is present due to separation from the head and helmet. The two large areas of low velocity and high turbulence located at $x = 12$ cm, 38 cm and $z = 60$ cm is assumed to come from the separation from the lower back, thighs and hips. These are the areas contributing to the majority of the drag. It is expected that these areas would be larger for the other arm positions tested which would increase the size of the wake. Hence, a larger pressure drop which in turn yields greater drag values. This coincides well with the measured force data.

As one can see from the vector and contour plots in Figure 12 a), Figure 13 a) and Figure 14 a), the flow is not symmetric. Especially the vector plot on the right side of the model show less circulation for the u and w velocity components compared to the left hand side which shows the circulation and the orientation clearer. There is a possibility that this is a coincidence coming from the coarse grid. It could be that the points premarked was not perfectly symmetric about the center of the model leading to different locations of the samples and hence, different values on the two sides. When looking at the vorticity in the same figure it is evident that the same phenomenons are experienced on both sides of the model. However, the measured data have different values here as well. This further supports that it might be a premarking error as the data measured are of different values. On the other side, as this is complex flow over a model of a real person symmetric data about the center of the model might not be a likely outcome.

A source of error from the wake measurements is due to the Cobra Probe being manually moved between every measurement point. The set-up could have been twisted or altered at some time during the tests. These are precise measurements, and the orientation a few degrees off yields considerably changes in the results. The spot of each measurement was premarked, as described in Section 2.1. In addition, the Cobra Probe was fastened in a manner that it did not affect the angle of the probe. Nonetheless, this is a major source of error for the wake measurements as even small changes in angle affect the measurements greatly. Some of the most turbulent areas, behind the hips and buttocks, had I_{uvw} above the 30% that was described in Section 2.1. As a consequence, the data from these areas have a higher uncertainty. However, when looking at the measured wake as a whole, the results from these areas does not differ from what was expected when looking at the areas with I_{uvw} below 30%.

4.1. Comparison of experimental and simulation results

When comparing the experimental and simulation results in Table 1 it is evident that all the drag results from the simulation are of a lower value than what obtained during the wind tunnel testing. The frontal area measurements are also smaller meaning the 3D print is larger than the scan. This explains some of the differences between the experimental and simulation results. It is clear from Table 1 that the trends are similar as the baseline and hands behind torso are the positions yielding the lowest drag area, and arms down and arms out are the two postures with highest drag area. This is further supported by Figure 5 where one can see the difference in C_dA relative to the baseline position for the experimental and simulation data. Figure 5 illustrates that the drag area relative to the baseline position are of a lower value for the simulations compared to the experiment. Nonetheless, the simulations are giving good results for the different arm positions.

For the upper arms of the baseline position the separation points for the experiment and simulation look similar. Both Figure 6 a) and b) also show a later separation point of the arm at knee height with some lines of flow separation going towards the knee. The flow visualization in Figure 7 a) illustrate a clearer separation with the arc on the lower thigh than what is the case from the pressure distribution displayed in Figure 6 b). Nonetheless, there are dark blue lines from the simulation in the same areas as the flow separates in the experiment indicating the same phenomena.

By comparing the different results for the arms down along legs position from Figure 8 a) and b) it is clear that the separation point agrees well. The upper arm has a later separation which changes right before the elbow yielding earlier separation for the forearm. The shape of the separation line for the whole arm are near identical for the experiment and simulation, but it looks like the flow separates somewhat earlier in the experiment for the upper arm.

Figure 9 a) and b) displays the flow separation point for the arms out position. Once again, the results from the simulation and experiment is in agreement. The same shape of the separation is seen in both figures. A later separation for the upper arm which turns into earlier separation from around the elbow until the wrist.

The position with hands behind the ankles show more deviating results between the simulation and experiment than the previous arm positions. As can be seen in Figure 10 a) and is discussed in Section 3.2, this arm position seems to be subject of both laminar and turbulent separation, and turbulent reattachment of the flow. This makes the comparison more difficult as the turbulence model used for the simulation assumes isotropic turbulence as discussed in Section 2.2. As a consequence, laminar separation and turbulent reattachment can not be seen from the simulation results. Figure 10 a) displays what looks like a later separation point for the upper arm and considerably earlier for the forearm compared to Figure 10 b).

Finally, the hands behind torso position experience some of the same flow phenomena as discussed in the last paragraph, but to a smaller extent. Figure 11 a) and b) have a similar separation line for the upper arm until just before the elbow. For the model in the wind tunnel, a case of both laminar and turbulent separation on the lower arm and just above the elbow was observed. On surface of the simulation model, it occurred more dark blue lines of low pressure making it difficult to decide exactly where the flow separates. If following the line of separation from the elbow and looking at the latest, turbulent separation of the experiment the lines coincide quite well.

Figure 16 a) and b) compares the experimental results with simulation results for the streamwise velocity component (v) in the wake of the baseline position. Figure 16 a) is identical with Figure 16 b), but with the experimental results added inside the black

square. This is the same area where the wake measurements were done in the wind tunnel. The same is done in Figure 17 a) and b) with turbulence intensity. The figures illustrate that the results are not identical for the two different cases, but they are similar and show the same trends. There is a large area with lower velocity and higher turbulence intensity located around the center for both the wind tunnel experiment and CFD simulation. The experimental results show higher velocity and lower turbulence in this area compared to the simulation. However, these are still low values of velocity and high values of turbulence for the experiment. It is clear that the simulation results from the wake is more asymmetric than what is the case for the experimental results. The reason for this is not known, but as described in Section 2.1 even a small change in which angle the model is tested at yields different results. When doing simulations, it is easy to orient the model exactly towards the incoming flow, but when doing measurements in the wind tunnel it is more difficult. Even though the placement and orientation of the model was decided with several reference measurements, it is possible that either the model or the force balance could have small offsets in angle influencing the results. Another issue is the resolution of the grid in Figure 3 where the Cobra Probe was used for measurements. Having larger distances of the sample points in the areas where the most turbulence occurs makes it harder to capture the smaller changes in the wake. It is plausible that by doing the exact same measurements with more points would yield a more asymmetric wake than what is the case for Figure 12 a), 13 a), 16 a), and 17 a).

Above this large area there is a small, white strip for both Figure 16 a) and b) and 17 a) and b). This is more or less identical for both the experiment and simulation, and is located towards the right with a larger area on top of the small strip.

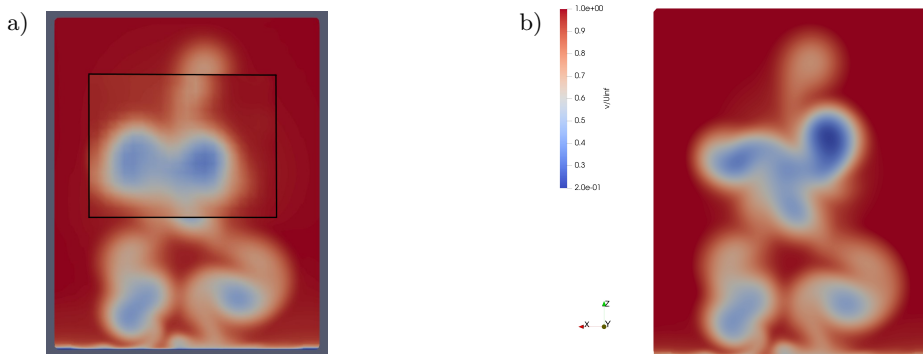


Figure 16: a) Experimental results (inside the black square) of the streamwise velocity component (v) on top of simulation results. b) Streamwise velocity component (v) from the simulation.

The comparison between the experimental and simulation results of the large-scale wake structures is based on Figure 14 a) for the experimental results and the upper half of Figure 14 b) for simulation results. First, the blue areas with CW vortices with large negative values will be discussed. It is clear that the larger blue area in the simulation is connected all the way, while the blue areas have a spacing between them with vorticity closer to 0 for the experiment. It seems like the larger values of negative vorticity for the simulation is located to the lower right whereas for the experiment it is located to the higher left. From both Figure 14 a) and b), it can be seen that the larger areas of CW vortices is located somewhat higher to the left above the red area, and below the red area to the right. This is a good indication for the CFD model. The blue areas also wrap

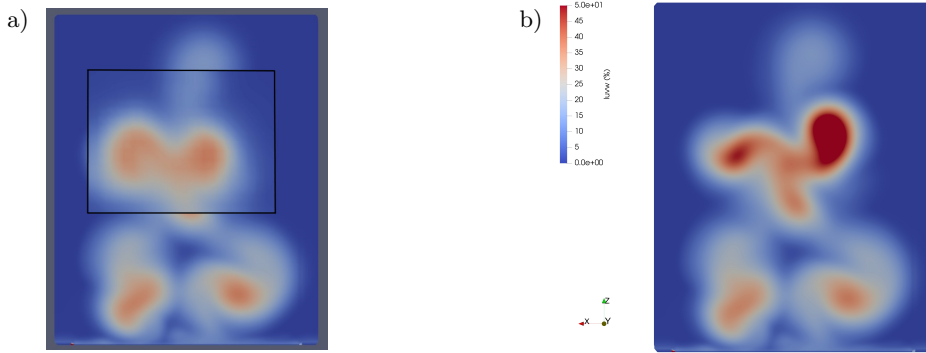


Figure 17: a) Experimental results (inside the black square) of the turbulence intensity (I_{uvw}) on top of simulation results. b) Principal turbulence intensity (I_{uvw}) from the simulation.

more around the red areas on the right side at around $z = 60$ cm for both the cases. In addition, both Figure 14 a) and b) show a blue area above these larger areas at around $z = 80$ cm from the helmet and head.

The red areas have CCW rotating vortices with large positive values. When looking at the upper half of Figure 14 b) from the simulation red areas are shown primarily as two large circles. One somewhat higher to the right, above the blue area, and the other one to the lower left. In addition, there are to smaller areas of CCW rotating vortices. One towards the top of the figure, coming from the head and helmet, and one in the lower, center of the upper half right below the largest blue area. From Figure 14 a) it is clear that the results obtained from the experiment have many of the same features as the simulation. There are to large, red, CCW rotating vortices present. One somewhat higher to the right center at $x = 35$ cm and $z = 65$ cm, and the other one lower to the left at $x = 15$ cm and $z = 55$ cm, just as in the simulation. It is also clear that in the lower part of the figure, at around $x = 38$ cm, there is a small part of a vortex in red. This was also seen in Figure 14 b). The only phenomenon missing is the vortex high in the figure on the left side of the blue vortex at $z = 80$ cm.

To summarize, both the experimental and simulation figures illustrates the same trends. There are some differences regarding the magnitude of the phenomenons and exactly how large the areas are, but the same trends are showing. As previously discussed, this could be due to the orientation towards the freestream flow or the number of measurement points in the grid. These are important findings for validating the digital wind tunnel. It would make it easier to do more tests than if dependent on the athletes and wind tunnel time. More arm positions could be tested for each athlete individually. It could also serve as a helpful tool when designing new suits where different fabrics and alterations to different parts of the suits could be tested depending on the flow around the separate body parts. In addition, more knowledge on flow around and in the wake of athletes with different arm positions can be obtained.

5. Conclusion

In this study, the effect of five different arm positions on flow around an alpine skier have been tested. Drag areas and flow separation points have been studied for all the arm positions. In addition, the streamwise velocity component, turbulence intensity and vorticity was investigated for the low tuck position in alpine skiing. A wind tunnel

experiment was conducted where drag measurements, flow visualizations with oil and wake measurements with Cobra Probe were done. The results from the experiment were compared with CFD simulations where drag forces, pressure distribution to find the flow separation points and wake data were obtained.

The ideal arm position for alpine skiers with regards to aerodynamic drag area (C_dA) is the low tucked baseline position, with arms down along the legs being the worst. During jumps it would be better for the athletes to have the arms out than along the legs. An even better position is the hands behind legs position, which would be a small change for the athletes compared to the arms down position. There are several reasons for the different values of C_dA for the arm sets. For one, the frontal area differ. The flow separation point is another fluid phenomenon affecting the drag later separations point yields a smaller wake which has a smaller pressure drop causing less pressure drag. The lower arms of the baseline position is a contributor as well as they are oriented towards the freestream, penetrating the air better and bending the flow around the upper arms yielding a later separation point. Finally, the flow characteristics in the wake is studied to gain knowledge on what is happening behind the model in the different arm positions. This study looked at the low tuck position with clockwise- and counterclockwise-rotating vortices being identified along with low velocity and high turbulence regions as large contributors to the drag.

The results obtained from the experiment in this study have several important applications. The drag measurements can be used by teams and athletes to shape off hundredths of seconds when jumping by holding the best possible arm positions with regards to drag area. In addition, it is possible to use the data on flow separation points and wake measurements when designing new racing suits. Finally, the results obtained from the flow visualization and wake measurements will serve as significant findings with respect to increasing the knowledge on the field of aerodynamics in alpine skiing.

This paper also serves as validation for a digital wind tunnel currently made by Nabla Flow. The simulation and experimental results were in good agreement for both characteristic flow regimes and large-scale flow structures. The figures were not identical when compared, but they were similar giving useful results for further developments of the CFD model used. In addition, the separation points from the flow visualization in the wind tunnel and the pressure distribution from the simulation compared well indicating that the digital wind tunnel captures complex flow phenomena satisfactory.

5.1. *Further work*

It would be of great interest to repeat the wake measurements with an automatic traverse for all the arm positions. The automatic traverse would do the testing less time consuming, making it possible to do the entire wake behind the model. The grid could also be finer with more measurement points for the same area in the wake. It would also be possible to do wake measurements at different lengths behind the model to see how the wake develops downstream. In addition, the uncertainties would be smaller compared to the manual traversing as the screw operation between every measurement is removed. When doing wake measurements of the different arm positions it is possible to see exactly what is causing the different drag forces in addition to the frontal area. Whether it is wake size, how symmetric the flow is, or strength of the vortices.

To do flow visualizations with oil on the entire body is also of interest. By doing this, one could see if the flow separates differently on the thighs and hips for the different arm positions. This would form more detailed figures of the wake characteristics, and further support the findings in this study.

REFERENCES

- ACHENBACH, E. 1971 Influence of surface roughness on the cross-flow around a circular cylinder. *Journal of Fluid Mechanics* **46** (2), 321–335.
- ACHENBACH, E. 1975 Total and local heat transfer from a smooth circular cylinder in cross-flow at high reynolds number. *International Journal of Heat and Mass Transfer* **18** (12), 1387–1396.
- ANDERSON, J.D. 2010 *Fundamentals of Aerodynamics*. McGraw-Hill Education.
- ANTHOINE, J., OLIVARI, D. & PORTUGAELS, D. 2009 Wind-tunnel blockage effect on drag coefficient of circular cylinders. *Wind and Structures* **12**.
- ASAI, T., HONG, S. & IJUIN, K. 2016 Flow visualization of downhill ski racers using computational fluid dynamics. *Procedia Engineering* **147**, 44–49.
- BARDAL, L.M. & REID, R. 2012 Testing of fabrics for use in alpine ski competition suits. *Procedia Engineering, Engineering of Sport Conference 2012* **34**, 44–49.
- BARELLE, C., RUBY, A. & TAVERNIER, M. 2004 Experimental model of the aerodynamic drag coefficient in alpine skiing. *Journal of Applied Biomechanics* **20**, 167–176.
- BATTISTI, L., ZANNE, L., DELL'ANNA, S., DOSSENA, V., PERSICO, G. & PARADISO, B. 2011 Aerodynamic measurements on a vertical axis wind turbine in a large scale wind tunnel. *Journal of Energy Resources Technology* **133**.
- BEARMAN, P.W. 1969 On vortex shedding from a circular cylinder in the critical Reynolds number régime. *Journal of Fluid Mechanics* **37** (3), 577–585.
- BIERMANN, D. & HERRNSTEIN JR., W.H. 1933 The interference between struts in various combinations. *National Advisory Committee for Aeronautics, Technical Report* p. 468.
- BROWNLIE, L. 2020 Aerodynamic drag reduction in winter sports: The quest for “free speed”. *Proceedings of the Institution of Mechanical Engineers, Part P: Journal of Sports Engineering and Technology*.
- CARBÓ MOLINA, A., DE TROYER, T., MASSAI, T. AND VERGAERDE, A., RUNACRES, M. & BARTOLI, G. 2019 Effect of turbulence on the performance of VAWTs: An experimental study in two different wind tunnels. *Journal of Wind Engineering and Industrial Aerodynamics* **193**.
- CROUCH, T., BURTON, D., BROWN, N., THOMPSON, M. & SHERIDAN, J. 2014 Flow topology in the wake of a cyclist and its effect on aerodynamic drag. *Journal of Fluid Mechanics* **748**, 5–35.
- DRASKOVIC, N. 2017 Measurement methods in turbulent flows. Master’s thesis, NTNU.
- ELFMARK, O. & BARDAL, L.M. 2018 An empirical model of aerodynamic drag in alpine skiing. *Proceedings* **2**, 310.
- ELFMARK, O., GILJARHUS, K.E., LILAND, F., OGGIANO, L. & REID, R. 2021 Aerodynamic investigation of tucked positions in alpine skiing. *Journal of Biomechanics* **119**.
- ELFMARK, O., REID, R. & BARDAL, L.M. 2020 Blockage correction and Reynolds number dependency of an alpine skier: A comparison between two closed-section wind tunnels. *Proceedings* **49**, 19.
- FEDEROLF, P., SCHEIBER, P., RAUSCHER, E., SCHWAMEDER, H., LÜTHI, A., RHYNER, H. & MÜLLER, E. 2008 Impact of skier actions on the gliding times in alpine skiing. *Scandinavian journal of medicine & science in sports* **18**, 790–7.
- HORI, E. 1959 Experiments on flow around a pair of parallel circular cylinders. *Proceedings of 9th Japan National Congress for Applied Mechanics* **3**, 231.
- LUETHI, S. & DENOTH, J. 1987 The influence of aerodynamic and anthropometric factors on speed in skiing. *International Journal of Sport Biomechanics* **3**, 345–352.
- MALLIPUDI, S., SELIG, M. & LONG, K. 2004 Use of a four hole cobra pressure probe to determine the unsteady wake characteristics of rotating objects.
- MASKELL, E.C. 1965 *A Theory of the Blockage Effects on Bluff Bodies and Stalled Wings in a Closed Wind Tunnel. Reports and memoranda*. H.M. Stationery Office.
- MEYER, F., LE PELLEY, D. & BORRANI, F. 2011 Aerodynamic drag modeling of alpine skiers performing giant slalom turns. *Medicine and science in sports and exercise* **44**, 1109–15.
- NABLAFLOW 2020 Digital wind, reinvented. <https://www.nablaflow.no/> Accessed on: 20.05.2021.
- OGGIANO, L., BROWNLIE, L., TROYNIKOV, O., BARDAL, L.M., SÆTER, C. & SÆTRAN, L. 2013 A review on skin suits and sport garment aerodynamics: Guidelines and state of the art. *Procedia Engineering* **60**, 91–98.

- SAVOLAINEN, S. & VISURI, R. 1994 A review of athletic energy expenditure, using skiing as a practical example. *Journal of applied biomechanics* **10**.
- SUPEJ, M., SÆTRAN, L., OGGIANO, L., ETTEMA, G., SARABON, N., NEMEC, B. & HOLMBERG, H.C. 2012 Aerodynamic drag is not the major determinant of performance during giant slalom skiing at the elite level. *Scandinavian journal of medicine & science in sports* **23**.
- WATANABE, K. & OHTSUKI, T. 1977 Postural changes and aerodynamic forces in alpine skiing. *Ergonomics* **20**, 121–131.
- WEST, G. & APELT, C. 1982 The effects of tunnel blockage and aspect ratio on the mean flow past a circular cylinder with Reynolds numbers between 10^4 and 10^5 . *Journal of Fluid Mechanics* **114**, 361 – 377.
- ZDRAVKOVICH, M.M. 1997 *Flow Around Circular Cylinders: Volume I: Fundamentals. Flow Around Circular Cylinders: A Comprehensive Guide Through Flow Phenomena, Experiments, Applications, Mathematical Models, and Computer Simulations*. OUP Oxford.
- ZDRAVKOVICH, M.M. & PRIDDEN, D.L. 1977 Interference between two circular cylinders; series of unexpected discontinuities. *Journal of Wind Engineering and Industrial Aerodynamics* **2** (3), 255–270.
- ZHOU, Y., WANG, Z. J., SO, R. M. C., XU, S. J. & JIN, W. 2001 Free vibrations of two side-by-side cylinders in a cross-flow. *Journal of Fluid Mechanics* **443**, 197–229.

Appendix A.

Appendix A includes blockage corrected and uncorrected C_dA , and blockage corrected and uncorrected C_d values for all the Re tested in the wind tunnel.

Table 2: The values for frontal area, uncorrected and corrected drag area, and uncorrected and corrected drag coefficient calculated for $U_\infty = 18$ m/s, equivalent to $Re = 5.60 \cdot 10^5$.

Arm position	Frontal area [m ²]	Uncorrected C_dA [m ²]	Corrected C_dA [m ²]	Uncorrected C_d [-]	Corrected C_d [-]
Baseline	0.266	0.185	0.170	0.694	0.640
Arms down	0.329	0.291	0.257	0.886	0.782
Arms out	0.340	0.254	0.228	0.748	0.671
Behind ankles	0.299	0.238	0.215	0.796	0.719
Behind torso	0.293	0.198	0.182	0.675	0.612

Table 3: The values for frontal area, uncorrected and corrected drag area, and uncorrected and corrected drag coefficient calculated for $U_\infty = 16$ m/s, equivalent to $Re = 5.00 \cdot 10^5$.

Arm position	Frontal area [m ²]	Uncorrected C_dA [m ²]	Corrected C_dA [m ²]	Uncorrected C_d [-]	Corrected C_d [-]
Baseline	0.266	0.196	0.180	0.737	0.677
Arms down	0.329	0.299	0.264	0.910	0.801
Arms out	0.340	0.263	0.235	0.773	0.691
Behind ankles	0.299	0.246	0.221	0.823	0.740
Behind torso	0.293	0.204	0.187	0.696	0.637

Table 4: The values for frontal area, uncorrected and corrected drag area, and uncorrected and corrected drag coefficient calculated for $U_\infty = 14$ m/s, equivalent to $Re = 4.40 \cdot 10^5$.

Arm position	Frontal area [m ²]	Uncorrected $C_d A$ [m ²]	Corrected $C_d A$ [m ²]	Uncorrected C_d [-]	Corrected C_d [-]
Baseline	0.266	0.212	0.193	0.797	0.727
Arms down	0.329	0.322	0.281	0.978	0.854
Arms out	0.340	0.276	0.245	0.812	0.721
Behind ankles	0.299	0.259	0.232	0.866	0.775
Behind torso	0.293	0.216	0.197	0.737	0.671

Table 5: The values for frontal area, uncorrected and corrected drag area, and uncorrected and corrected drag coefficient calculated for $U_\infty = 12$ m/s, equivalent to $Re = 3.70 \cdot 10^5$.

Arm position	Frontal area [m ²]	Uncorrected $C_d A$ [m ²]	Corrected $C_d A$ [m ²]	Uncorrected C_d [-]	Corrected C_d [-]
Baseline	0.266	0.233	0.211	0.877	0.794
Arms down	0.329	0.339	0.294	1.030	0.893
Arms out	0.340	0.302	0.266	0.888	0.781
Behind ankles	0.299	0.277	0.246	0.925	0.822
Behind torso	0.293	0.237	0.214	0.810	0.731

Table 6: The values for frontal area, uncorrected and corrected drag area, and uncorrected and corrected drag coefficient calculated for $U_\infty = 10$ m/s, equivalent to $Re = 3.10 \cdot 10^5$.

Arm position	Frontal area [m ²]	Uncorrected $C_d A$ [m ²]	Corrected $C_d A$ [m ²]	Uncorrected C_d [-]	Corrected C_d [-]
Baseline	0.266	0.263	0.235	0.987	0.882
Arms down	0.329	0.362	0.311	1.100	0.946
Arms out	0.340	0.330	0.287	0.969	0.843
Behind ankles	0.299	0.303	0.267	1.013	0.892
Behind torso	0.293	0.267	0.238	0.912	0.813